Light-Induced Photochemical Changes in Copper(I) Thiocyanate Complexes Decorated with Halopyridines: Optical Memory Manifestation

Aaron D. Nicholas

Brooke M. Otten

Gerardo Ayala

et al.

Robert D. Pike

Light-Induced Photochemical Changes in Copper(I) Thiocyanate Complexes Decorated with Halopyridines. Optical Memory Manifestation

Aaron D. Nicholas,[a] Brooke M. Otten,[b] Gerardo Ayala,[c] James Hutchinson,[a] Lukasz Wojtas,[d] Mohammad A. Omary,[b*] Robert D. Pike,[c] and Howard H. Patterson[a*]

[a]*Department of Chemistry, University of Maine, Orono, ME 04469,* [b]*Department of Chemistry, University of North Texas, Denton, TX, 76203,* [c]*Department of Chemistry, College of William and Mary, Williamsburg, VA 23187,* [d]*Department of Chemistry, University of South Florida, Tampa, FL 33620.*

*Corresponding Authors: Email: howardp@maine.edu (H.H.P.); omary@unt.edu (M.A.O.)

Abstract

We report on the photoluminescence of $\{CuSCN(3\text{-}XPy)_2\}_n$ crystals (X = Br, Cl; Py = pyridine). Laser excitation at 266 nm for $CuSCN(3\text{-}BrPy)_2$ at 78 K results in a decrease in the luminescence intensity with increasing irradiation time. Heating the sample to 298 K and re-cooling to 78 K results in recovery of the original luminescence intensity, hence manifesting an optical memory effect. Laser irradiation at longer or shorter wavelengths fails to produce a reduction in emission intensity. Interestingly, $CuSCN(3\text{-}ClPy)_2$, despite being isomorphic, does not undergo emission intensity changes regardless of laser irradiation wavelength variation. Density Functional Theory (DFT) and Time Dependent DFT (TD-DFT) calculations were performed on an adjacent chain model to explore the photochemical change that occurs upon laser irradiation. The observed reduction in luminescence intensity is attributed to photo-induced electron transfer quenching in which Cu(I) is oxidized to a non-luminescent Cu(II) with capture of the halogen by a neighboring SCN ligand on the adjacent coordination polymer chain.

1.   Introduction

Optical memory-based data storage has the potential to replace current methods as a durable and inexpensive storage medium.[1-3] However, the lack of viable materials has hindered the development of such devices.[1-3] Optical memory based on luminescence is a phenomenon in which a solid-state chemical compound undergoes a reversible photophysical or photochemical change at low temperatures as the result of laser irradiation.[5-7] This change produces luminescence properties that differ from those prior to irradiation. Information can thus be "written" onto the chemical compound through irradiation, which alters the crystal structure. Data "write" operations are thus enabled via alteration in the luminescence emission behavior. Heating the compound to ambient temperature and subsequently recooling reverses the change. This recovery sequence effectively "erases" the memory of the crystal structure. As a result, compounds that exhibit a complete write/erase cycle have great potential for data storage.

Early optical metal systems consisting of Cu^+/Ag^+ doped β''-Alumina were first reported by Zink et al.[4] The mechanism reported by Zink shows that emission initially results from Cu^+/Cu^+ dimers but changes to Cu^+/Ag^+ dimers after laser irradiation at 78 K.[4] Interestingly, these coordination complexes of Cu(I) salts were shown to exhibit optical memory properties, based on their ability to reversibly undergo a metal cluster structural alteration in response to exposure to high-energy electromagnetic radiation.[4] Non-irradiated regions continue to show emission bands associated with Cu^+/Cu^+ dimers, demonstrating that the reduction in emission results from a photophysical change rather than a photochemical change.[4] Following the work by Zink et al., we previously reported on the luminescence phenomenon of optical memory for crystals of $Pb(Au(CN)_2)_2$.[8] Upon exposure to 337 nm laser irradiation at 78 K this complex also undergoes a drastic reduction in emission intensity as a function of irradiation time. Unlike the photophysical

change reported by Zink, we concluded that this decrease in emission was the result of photoinduced electron transfer. In this transfer the $Au(CN)_2^-$ ligands in the excited state oxidize the coordinated Pb^{2+} to Pb^{4+} and eventually decompose to Au and CN^-. At low temperatures Au and CN^- formation is irreversible, preventing back electron transfer to the original state. However, upon heating to room temperature this process becomes reversible and the complex emission is fully recovered to pre-irradiation intensities.

More recently, we have published optical memory results for similar systems which show a photo-induced electron transfer mechanism.[4-7] Interestingly, systems displaying photophysical changes rather than photochemical changes have also been reported. We have reported optical memory behavior in layered crystals of $K_2Na[Ag(CN)_2]_3$.[7,9-11] We used a pure, undoped crystalline complex of Ag(I) to produce new oligomeric excimers upon irradiation.[3] Optical memory behavior for this system was seen through the reduction of both a high-energy emission band and a low-energy band upon 266 nm laser irradiation.[7,9-11] At low temperatures, high-emission-energy Ag-Ag* dimers convert into low-emission-energy linear silver trimers at 402 nm, Ag-Ag-Ag*.[7] However, as these linear trimers are irradiated, they undergo a photophysical change into excited state bent trimers, resulting in reduced emission intensity of the 402 nm linear trimer band and appearance of a new 380 nm band assigned to a bent trimer. Heating of the crystalline sample results in recovery of the emission spectrum to its original state.

Herein, we report an investigation of the optical memory properties of $CuSCN(3\text{-}XPy)_2$ crystals (X = Br, Cl; Py = pyridine) which exhibit broad emission bands in the visible region. These bands are assigned to a metal-to-ligand charge transfer (MLCT) in which electrons are transferred from the $(CuSCN)_\infty$ chain backbone to the pyridine ring. Laser irradiation at 266 nm of $CuSCN(3\text{-}BrPy)_2$ held at 78 K results in significant reduction in emission intensity over time.

This decrease is reversed by heating the sample to 298 K and recooling to 78 K. Laser irradiation of CuSCN(3-ClPy)$_2$ while held at 78 K produces no change in the luminescence intensity. We model the reduction for emission intensity of CuSCN(3-BrPy)$_2$ as a photo-induced electron transfer in which Cu(I) is oxidized to a non-luminescent Cu(II) with capture of the halogen by the neighboring SCN ligand on an adjacent chain.

2. Experimental

2.1 Preparation of Compounds

Crystals of **1** and **2** were prepared according to a modification of our previously reported method.[12] Solid CuSCN (100 mg, 0.822 mmol) was stirred with an excess of neat 3-halopyridine ligand in sealed vials under Ar for 4 days, forming the products as bulk powders in suspension. The sealed vials were then heated to 70 °C in an oil bath for 2 h without stirring. The resulting solutions were then allowed to slowly cool to room temperature. Pale yellow crystals were collected by decanting the green supernatant, washing the solid with neat ligand, and then with ethyl ether, before air-drying. Yields: CuSCN(3-BrPy)$_2$ = 311 mg, 0.711 mmol, 86.5%, CuSCN(3-ClPy)$_2$ = 226 mg, 0.648 mmol, 78.8%. Copper analysis was carried out by atomic absorption spectroscopy after acid digestion.[13] Anal. Calcd for C$_{11}$H$_8$Br$_2$CuN$_3$S: C, 30.19; H, 1.84; N, 9.60; Cu, 14.52. Found: C, 29.60; H, 1.80; N, 9.50; Cu, 15.01. Calcd for C$_{11}$H$_8$N$_3$Cl$_2$CuS: C, 37.89; H, 2.31; N, 12.05; Cu, 18.22. Found: C, 37.40; H, 2.26; N, 11.99; Cu, 17.73.

2.2 X-ray Analysis

Single crystal determinations were carried out using a Bruker SMART Apex II diffractometer using graphite-monochromated Cu Kα radiation.[14a] The data were corrected for Lorentz and polarization effects and absorption using SADABS.[14b,c] The structures were solved

by use of intrinsic phasing. All crystals for both compounds were found to be pseudomerohedrally twinned with orthorhombic *C* symmetry. Data were solved and refined with monoclinic *P* symmetry as a two-component twin (twin law = 1 0 0 / 0 –1 0 / –1 0 –1) with 2-fold axis along [100] direction as a twin operator. The two structures were isomorphic and solved as enantiomorphs (see Electronic Supporting Information, SI). Least squares refinement on F^2 was used for all reflections. Structure solution, refinement and the calculation of derived results were performed using the SHELXTL package of software.[14c] The non-hydrogen atoms were refined isotropically. In all cases, hydrogen atoms were placed in theoretical positions. X-ray refinement details for all structures are summarized in Table 1.

Table 1. Crystal and structure refinement data

	1	2
CCDC deposit no.	1483473	1483474
color and habit	yellow block	yellow prism
size, mm	$0.28 \times 0.23 \times 0.10$	$0.52 \times 0.15 \times 0.14$
formula	$C_{44}H_{32}Br_8Cu_4N_{12}S_4$	$C_{44}H_{32}Cl_8Cu_4N_{12}S_4$
formula weight	1750.49	1394.81
space group	*Pc* (#7)	*Pc* (#7)
a, Å	11.5742(2)	11.4848(2)
b, Å	9.4358(2)	9.2543(2)
c, Å	25.9158(5)	25.8293(5)
β, deg	102.9110(10)	102.8390(7)
volume, Å^3	2758.76(9)	2676.59(9)
Z	2	2
ρ_{calc}, g cm^{-3}	2.107	1.731
F_{000}	1680	1392
μ(Cu Kα), mm^{-1}	10.310	7.303
temperature, K	100	100
residuals:[a] R; R$_w$	0.0303; 0.0797	0.0395; 0.0987
goodness of fit	1.044	1.032

[a]R = R_1 = $\Sigma||F_o| - |F_c||/ \Sigma|F_o|$ for observed data only. R$_w$ = wR_2 = $\{\Sigma[w(F_o{}^2 - F_c{}^2)^2]/\Sigma[w(F_o{}^2)^2]\}^{1/2}$ for all data.

*2.3 Steady-State Luminescence and Optical Memory Measurements*

Steady-state luminescence scans were recorded at 298 K and 78 K. Spectra were taken with a Model Quantamaster-1046 photoluminescence spectrophotometer from Photon Technology International using a 75W xenon arc lamp combined with two excitation monochromators and one emission monochromator. A photomultiplier tube at 800 V was used as the emission detector. Emission intensity was corrected for variation in lamp intensity. The solid samples were mounted on a copper plate using non-emitting copper-dust high vacuum grease. All scans were run under vacuum using a Janis ST-100 optical cryostat. Low temperature scans used liquid nitrogen as coolant. Laser irradiation occurred with an Opolette Model 355II and UV tunable pulse laser using a Nd:Yag laser pump. Laser power output at each wavelength is summarized in Table S1 (SI). All luminescence scans were collected with a 5-nm excitation and emission slit width. Focusing lenses were initially adjusted prior to irradiation to maximize emission intensity for each compound. Samples were irradiated at 78 K for 5-minute intervals. Recovery measurements were accomplished by allowing samples to reach thermal equilibrium at 298 K before being cooled back to 78 K.

2.4 Computational Methodology

All geometry optimizations were performed using the Gaussian09 software program.[15] Calculations were performed using the M06 meta-hybrid functional[16a,b] with the CEP-31G(d) basis set.[16c,d] To determine the most accurate model, we calculated the ground and excited state geometries of three primary monomer units with corresponding dimers and trimers at the B3LYP[17,18] and M06 level of theory (SI).[16a,b] Appropriate monomer and dimer/oligomer models were used that account for the correct geometry and coordination number of the metal center(s) as in the pertinent crystal structure in the input files of all DFT and TD-DFT computations, including ground- and excited-state single-point and full or partial (scan) geometry optimization. The three

basic monomer units employed, shown in Scheme I, were a neutral three coordinate copper model

of formula CuSCN(3-XPy), a four coordinate metal anion model of formula [Cu(SCN)(SCN)(3-

XPy)$_2$]$^-$ and a four coordinate metal neutral model of formula Cu(SCNH)(SCN)(3-XPy)$_2$.

Scheme I. Schematic showing the three basic monomer units explored for DFT and TD-DFT

calculations; (**A**) a neutral three coordinate copper model of formula CuSCN(3-BrPy), (**B**) a four

coordinate copper anion model of formula [Cu(SCN)(SCN)(3-XPy)$_2$]$^-$ and (**C**) a four coordinate

copper neutral model of formula Cu(SCNH)(SCN)(3-XPy)$_2$.
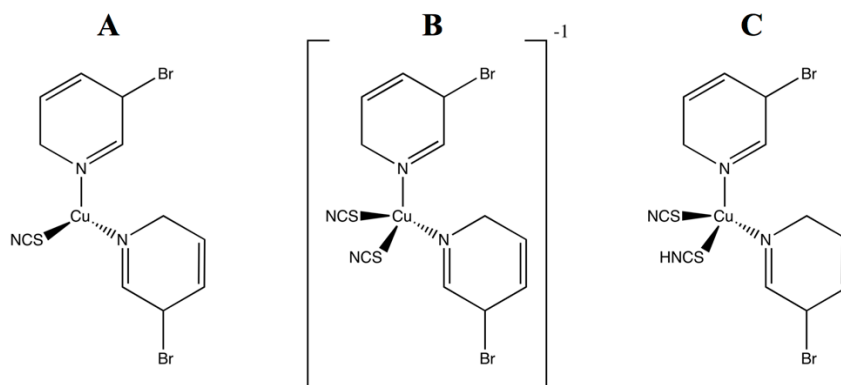
Calculated geometries, excitation energies, and emission energies were compared to experimental

results to identify the most accurate model. From this selection process we have identified the four

coordinate metal anion model of formula [Cu(SCN)$_2$(3-XPy)$_2$]$^-$ as the most accurate base

monomer unit. This unit was expanded into an adjacent-chain model which was then optimized in

the ground and excited state to provide insight into the geometric changes that occur in CuSCN(3-

XPy)$_2$ coordination polymer crystals upon laser irradiation.

3.   **Results and Discussion**

    3.1 Description of X-ray Structures

    3.1.1 Literature Context

        We have previously published a longitudinal structural study of Cu^{I}SCN complexes

coordinated with nitrogenous bases (L).[12] Compounds of the type Cu^{I}SCN(L) (1:1) are

common.[12,19,20] Structurally, these complexes form 2-D rippled sheet networks in which the μ_3-SCN ligand shows N, S, S coordination to three Cu(I) centers. The fourth of the tetrahedral coordination sites on each Cu(I) center is occupied by L. All angles around Cu(I) centers approximate tetrahedral, but the S–Cu–N_{CS} chain angle tends to be on the larger side. These reported 1:1 networks include $Cu^ISCN(3\text{-}XPy)$ (X = Cl, Br), which show chain angles of 116.2–117.5°. Compounds of the type $Cu^ISCN(L)_2$ (1:2), new examples of which are reported below, are also prevalent and form 1-D zigzag chains of $(Cu^ISCN)_\infty$ coordination polymers decorated with pairs of L at each roughly tetrahedral Cu(I) center. Chain angles tend to be slightly larger than tetrahedral. A single example of $Cu^ISCN(L)_3$ species, namely $Cu^ISCN(3\text{-}EtPy)_3$, is a tetrahedral monomer, whereas all others are coordination polymers.[12]

3.1.2 CuSCN(3-BrPy)₂

The compound $CuSCN(3\text{-}BrPy)_2$ crystallized as yellow prisms, solving in the polar monoclinic space group *Pc*. A structural diagram is shown in Figure 1, and selected bond lengths and angles are given in Table 2. The crystallographic repeat unit consists of two independent 1-D CuSCN chain segments. These chain segments each contain two independent CuSCN units decorated by pairs of 3-BrPy ligands coordinated at each metal center. The nominally tetrahedral angles about the copper centers range from 96.5(3)° to 115.3(2)°. Zigzag angles along the chains (N–Cu–S) are 111.6(3), 114.7(3), 111.5(3), and 115.3(2)°.

Table 2. Selected Bond Distances (Å) and Angles (°) for CuSCN(3-BrPy)₂ and CuSCN(3-ClPy)₂.

	CuSCN(3-BrPy)₂	CuSCN(3-ClPy)₂
Cu–N_{CS}	1.935(9), 1.942(9), 1.946(9), 1.963(9)	1.921(7), 1.950(7), 1.972(10), 1.974(9)
Cu–S_{CN}	2.295(3), 2.300(3), 2.331(3), 2.342(3)	2.286(3), 2.305(2), 2.328(3), 2.344(2)
Cu–N_{Py}	2.069(8), 2.087(8), 2.076(8), 2.101(7), 2.073(8), 2.087(8), 2.060(8), 2.098(8)	2.034(7), 2.050(7), 2.062(7), 2.068(8), 2.086(7), 2.091(7), 2.107(7), 2.115(7)
S–C	1.656(10), 1.673(10), 1.666(10), 1.659(10)	1.696(9), 1.699(9), 1.647(10), 1.641(9)

9

|		
C–N	1.157(14), 1.145(13), 1.158(13), 1.158(13)	1.092(12), 1.105(12), 1.155(12), 1.168(11)
$_{SC}$N–Cu–S$_{CN}$	111.5(3), 111.6(3), 114.7(3), 115.3(2)	109.9(3), 109.5(3), 113.6(2), 113.9(2)
$_{SC}$N–Cu–N$_{Py}$	105.6(3), 106.2(3), 110.7(3), 110.9(3), 111.0(3), 112.7(3), 113.3(3), 113.4(3)	105.4(3), 107.0(3), 110.0(3), 110.7(3), 112.3(3), 112.9(3), 113.3(3), 113.8(3)
$_{NC}$S–Cu–N$_{Py}$	106.0(2), 106.5(2), 106.5(2), 108.6(2), 113.4(2), 109.7(2), 107.7(2), 114.3(2)	105.72(19), 106.5(2), 107.7(2), 107.8(2), 108.1(2), 109.1(2), 113.8(2), 115.8(2)
N$_{Py}$–Cu–N$_{Py}$	110.2(3), 96.5(3), 111.1(3), 97.1(3)	96.4(3), 97.6(3), 111.1(3), 112.5(3)
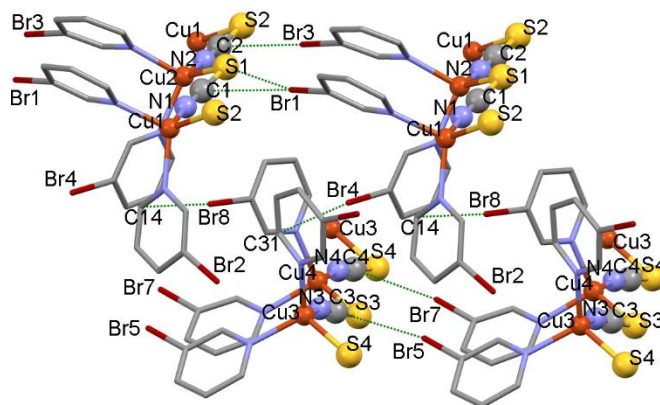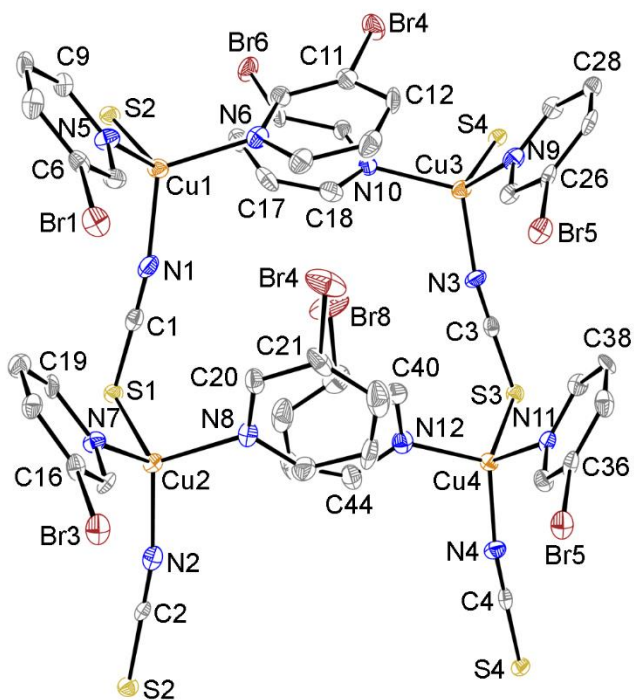
Figure 1. X-ray crystal structure of CuSCN(3-BrPy)$_2$. **Top**: 50% thermal ellipsoid drawing showing the crystallographically independent unit. **Bottom**: view along the chains showing close interactions. The 3-BrPy ligand is shown as wireframe and the CuSCN atoms as ball and stick. Hydrogen atoms have been omitted. Color scheme for X-ray structures: orange = Cu, grey = C, blue = N, yellow = S, dark red = Br, green = Cl.

As shown in Figure 1, one pair of bromopyridine molecules in the first chain, containing Br1 and Br3, is oriented in nearly identical direction, while the other pair, containing Br2 and Br4, is canted in nearly orthogonal direction relative to one another. The interplanar angle formed between the bromopyridines containing Br2 and Br4 is 87.30°. The same pattern is seen in the second chain, where Br5 and Br7 are canted in nearly identical directions, while the angle between the pyridines containing Br6 and Br8 is 87.14°. No π–stacking between any of the 3-BrPy ligands is evident. However, numerous interactions between the bromine atoms and neighboring thiocyanate units or pyridine rings are evident. Table 3 below summarizes these close Br···S and Br···C interactions.

Table 3. Close atom interactions for CuSCN(3-BrPy)$_2$ and CuSCN(3-ClPy)$_2$.

CuSCN(3-BrPy)$_2$			CuSCN(3-ClPy)$_2$		
Atom 1	**Atom 2**	**Distance (Å)**	**Atom 1**	**Atom 2**	**Distance (Å)**
Br1	C1 (SCN)	3.42(1)	Cl1	C1 (SCN)	3.329(8)
Br1	S1	3.614(2)	Cl3	C2 (SCN)	3.375(8)
Br2	C44 (BrPy)	3.49(1)	Cl6	C3 (SCN)	3.466(9)
Br3	C2 (SCN)	3.369(9)	Cl8	C4 (SCN)	3.294(8)
Br4	C34 (BrPy)	3.46(1)	C20 (ClPy)	C28 (ClPy)	3.22(1)
Br5	C3 (SCN)	3.46(1)	C23 (ClPy)	C29 (ClPy)	3.30(1)
Br6	C24 (BrPy)	3.47(1)	Cl4	H40 (ClPy)	2.882
Br7	C4 (SCN)	3.34(1)	S2	H37 (ClPy)	2.713
Br8	C14 (BrPy)	3.47(1)	S3	H12 (ClPy)	2.737

Noticeable differences in interactions between the Br and Cl complex are apparent in the orientations of Br1, Br3, Br5, and Br7 substituents in bromopyridine ligands. In the Br complex

the bromopyridine ligands point toward the thiocyanate groups of the neighboring chains with an average estimated distance of roughly 3.4 Å.

3.1.3 Structure of CuSCN(3-ClPy)$_2$

The compound CuSCN(3-ClPy)$_2$ also crystallized as yellow prisms, solving as an isomorph to CuSCN(3-BrPy)$_2$. As is the case for the 3-BrPy complex, four independent CuSCN(3-ClPy)$_2$ units are present, forming two distinct chains. Structural diagrams are shown in Figures 2 and S2 (SI), and selected bond lengths and angles are given in Table 2. The chain zigzag angles are 113.6(2), 109.9(3), 109.5(3), and 113.9(2)°. Table 2 summarizes the close atom interactions seen in this structure. Three chlorine atoms (Cl1, Cl3 and Cl8) showed close interactions of about 3.3 Å with thiocyanate carbon atoms. The distance Cl6···C4 = 3.466(9) Å falls just outside the van der Waals radius sum for a bonding interaction between carbon and chlorine (3.45 Å). As was the case for CuSCN(3-BrPy)$_2$, the chloropyridine rings containing Cl1 and Cl3 are canted in identical directions, resulting in the close Cl···C distances. The pyridine ligand pairs containing Cl2 and Cl4, along with those pairs containing Cl5 and Cl7, are canted in orthogonal directions, as was observed for CuSCN(3-BrPy)$_2$. The angles between the pairs of ligands are 86.52° and 86.03° respectively. These chlorines do not appear to have interactions with neighboring ring carbons, although the Cl4···H40 distance of 2.882 Å falls within the van der Waals radius sum of the two atoms. Similarly, S2···H37 and S34···H12 are close enough to indicate potential hydrogen bonding-like interactions.
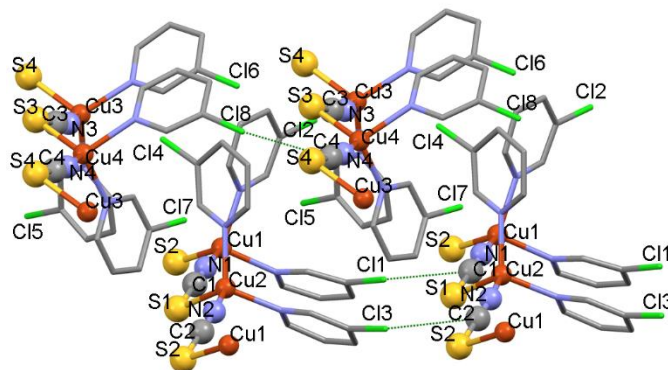
Figure 2. CuSCN(3-ClPy)$_2$ viewed along the chains showing close interactions between chlorine atoms and thiocyanate units.

3.2 Photoluminescence Spectra of CuSCN(3-XPy)$_2$ Manifesting Optical Memory

We have previously published the results on the solid state luminescence of a series of CuSCNL$_2$ complexes including CuSCN(3-BrPy)$_2$ and CuSCN(3-ClPy)$_2$.[12] A general overview of the luminescence band assignment is given here, whereas additional insights are provided in ref 12 and the computational sections below. The broad emission bands of these compounds are assigned as a MLCT. In these copper(I) compounds, aromatic ligands are required to produce luminescence wherein the lowest unoccupied molecular orbital (LUMO) has a π* character localized on the aromatic ligand that acts as an electron acceptor.[12] In CuCN systems, MLCT is possible through the electron-accepting nature of the cyanide group; however, the substitution of CN with SCN changes the electron-donating ability of the metal during excitation. Because luminescence behavior is highly dependent on the nature of the pyridine ring, substituent changes to the ring should result in dramatic changes in luminescence.

Optical memory results for CuSCN(3-BrPy)$_2$ in Figure 3 show a broad and high-intensity luminescence emission peak between 425–675 nm at 78 K consistent with previously published data.[12] Upon laser irradiation, the emission peak position remains unshifted. This compound shows a large reduction in emission intensity upon exposure to 266 nm laser irradiation. A maximum

reduction in intensity of 88% is reached after irradiation for 20 minutes. An emission reduction half-life of 7.52 min. is calculated. This reduction in intensity remains stable at 78 K over the time period observed, as illustrated in Figure S5 (SI). Warming the sample to 298 K and re-cooling to 78 K resulted in an emission spectrum nearly identical to that seen prior to irradiation with a recovery of 98%. Thus, recovery was found to be quantitative within experimental error. Two additional optical memory experiment cycles were performed to confirm optical memory recovery, as shown in Figure 3. Cycles 2 and 3 confirm the cycling ability of $CuSCN(3\text{-}BrPy)_2$ upon laser irradiation at 266 nm with recoveries of 108% and 103%, respectively; we consider the 98-108% recoveries to be quantitative, with the small variations being due to experimental error. The ability to recover the original emission behavior demonstrates a spontaneously reversible chemical change due to thermal energy. As seen in Figure 4, unlike the bromopyridine analog, $CuSCN(3\text{-}ClPy)_2$ exhibits no emission intensity reduction upon laser irradiation at wavelengths of 318 nm, 270 nm, 239 nm, and 210 nm. This absence of emission reduction indicates that the excited states at these energy levels are not connected with the photoluminescence of this compound. This result stands in stark contrast to the luminescence behavior observed with $CuSCN(3\text{-}BrPy)_2$.
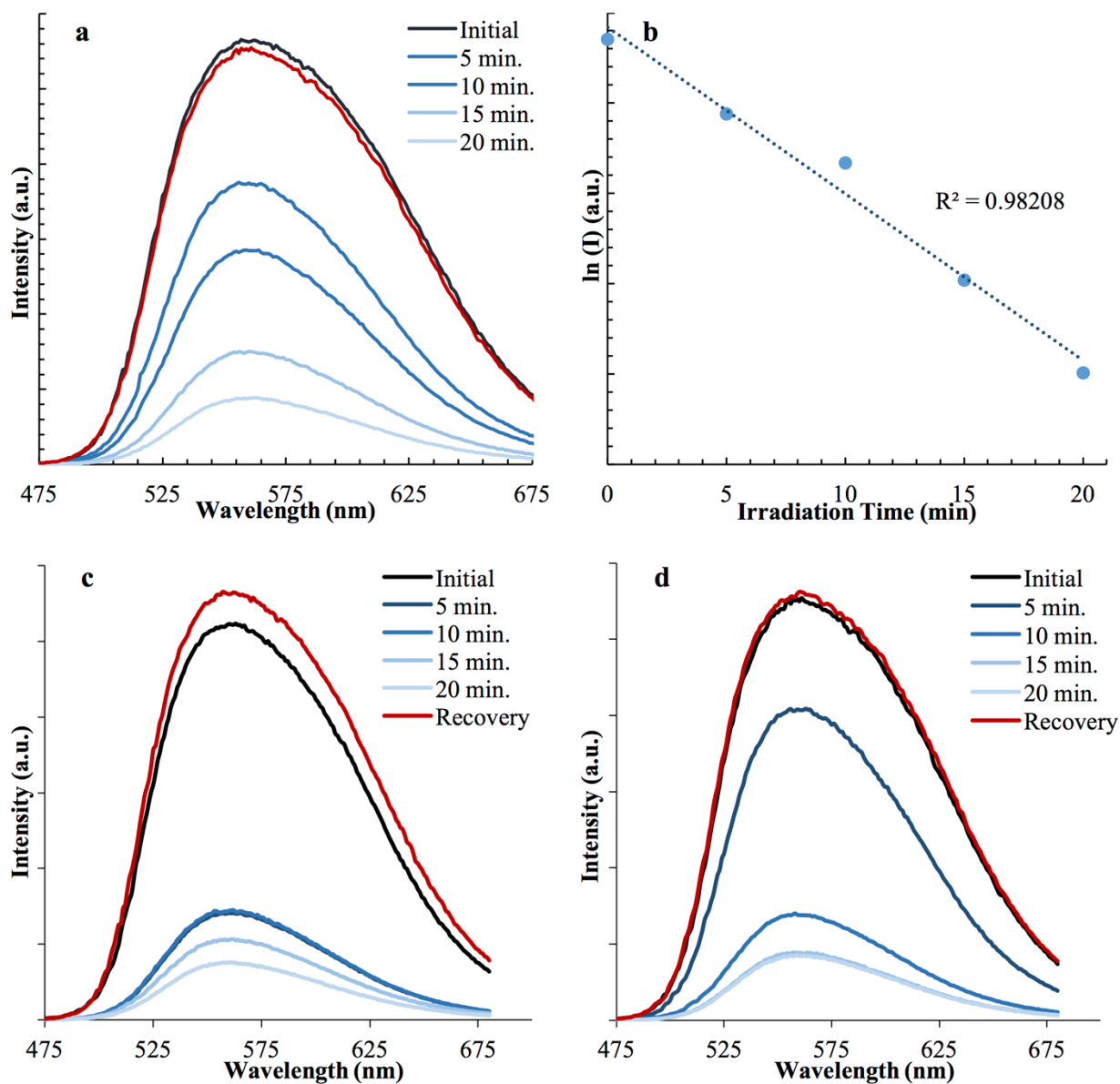
Figure 3. Emission spectra for (CuSCN)(3-BrPy)$_2$ after 5-minute intervals of (**a**) **266** nm and (**b**) variation in emission intensity with increasing laser irradiation for **266** nm excitation. Half-life of 7.52 min calculated. Cycle 2 (**c**) and cycle 3 (**d**) performed succession on sample crystal. All spectra obtained at 78 K.
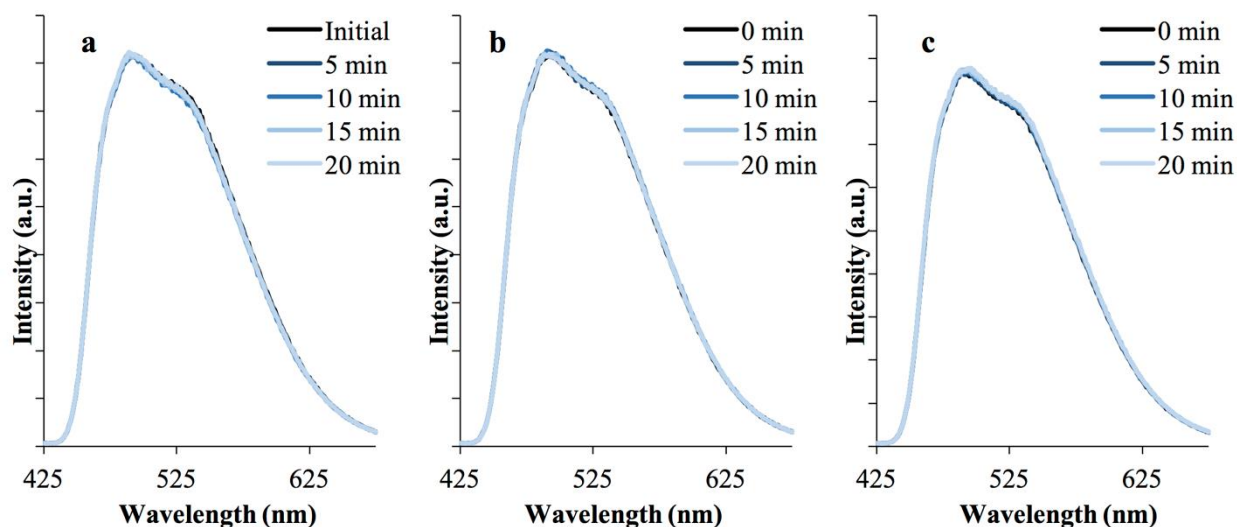
Figure 4a-c. Emission spectra for CuSCN(3-ClPy)$_2$ after 5 minute intervals of (**a**) **318** nm, (**b**) **270** nm, and (**c**) **239** nm laser irradiation. All spectra obtained at 78 K.

3.3 DFT Calculations of CuSCN(3-XPy)$_2$.

3.3.1.1 Ground State Geometry of CuSCN(3-BrPy)$_2$ and CuSCN(3-ClPy)$_2$.

To accurately model the experimental phenomena reported herein for CuSCN(3-BrPy)$_2$, an anionic, 4-coordinate adjacent-chain model was selected based on its ground state structural agreement with the crystal structure, as shown in Figure 5. There is good qualitative agreement not only in the coordination sphere of the Cu but also in the placement of the pyridine ligands to give the Cu center a tetrahedral geometry. The model also accounts for the Cu$\cdots$Cu distance of CuSCN(3-BrPy)$_2$, predicting a distance of 8.677 Å while the crystal structure shows a distance of 8.447 Å. The closest S$\cdots$Br distance in the model is predicted to be 4.3054 Å, which is 0.4 Å shorter than the crystal structure value. The differences in the bond angles and lengths from those in the crystal structure are attributed to the fact the calculations are performed in the gas phase and the units are monomers which do not account for oligomerization packing effects and weaker intra- and intermolecular interactions. DFT, and the selected basis set, have limitations when describing weak interactions.
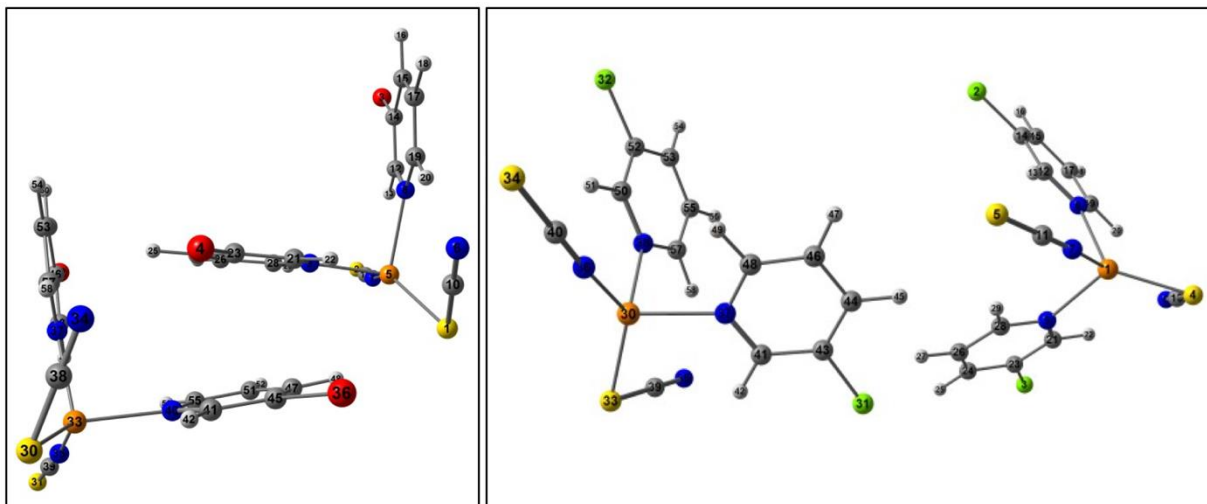
16

Figure 5. The M06/CEP-31G(d) optimized ground state structure for adjacent chains of (**left**) $\{[Cu(SCN)_2(3\text{-}BrPy)_2]\}_2^{-2}$ and (**right**) $\{[Cu(SCN)_2(3\text{-}BrPy)_2]\}_2^{-2}$.

It was also found that the adjacent chain model had the best structural agreement for the 4-coordinate, anionic model of CuSCN(3-ClPy)$_2$ (see Figure 5). As was with the CuSCN(3-BrPy)$_2$ complex, the differences in the bond angles are attributed to the fact the calculations are run in the gas phase. So while the adjacent chain model accounts for the packing effects of monomeric units, it does not account for the solid state packing of chains of oligomers, since DFT has limitations when describing weak interactions.

3.3.1.1 Excited State Geometries of CuSCN(3-BrPy)$_2$ and CuSCN(3-ClPy)$_2$.

The excited state geometry of the lowest triplet of Cu(SCN)$_2$(3-BrPy)$_2$ was also calculated and is shown in comparison to the ground state geometry below in Figure 6 and Table S5 (SI). Upon excitation, the pyridine stacking that is seen in the ground state is lost, and there is elongation of the Cu···Cu and S···Br distances. It also appears that the coordination sphere around the Cu center becomes closer to a trigonal planar geometry with the dissociation of one of the pyridine rings with the Cu–N bond distances lengthening to 2.5 and 3.5 Å.
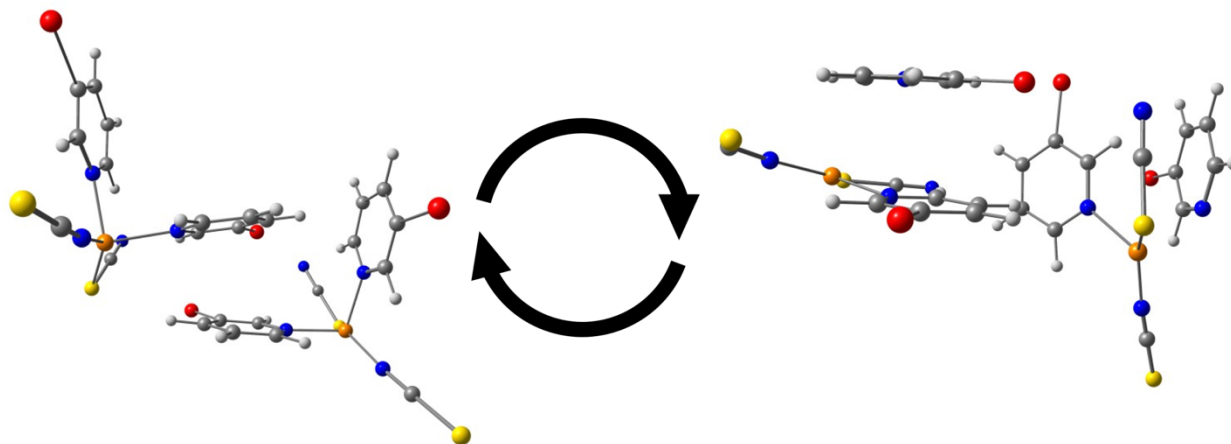
17

Figure 6. Ground state (S_0) and excited state (T_1) structures.

Given that the adjacent chain model of $Cu(SCN)_2(3\text{-}BrPy)_2$ gave the best structural agreement, this structure was used to perform TD-DFT calculations to model the excitation spectrum for this molecule. It was found that both the calculated and the experimental spectra (see SI) gave broad bands corresponding to MLCT states from the CuSCN backbone to the π^* of the aromatic ring. The orbitals corresponding to the transitions with the highest oscillator strength were mapped and used to determine the transition types. Orbital transitions (see SI) support the MLCT transition assignment wherein electron density from the CuSCN center are transferred to the aromatic π^* system.

In the case of $CuSCN(3\text{-}BrPy)_2$ optical memory behavior is dependent on irradiation energy. Only at 264 nm laser irradiation do we observe a reduction in luminescence intensity and full recovery. To probe why this specific irradiation energy gives this behavior we have performed a series of TD-DFT optimized excited state geometries corresponding to different laser irradiation wavelengths. A lower-energy triplet excited state A is calculated at 334 nm where laser irradiation (318 nm) does not result in a reduction in emission intensity. TD-DFT optimized geometry calculations for excited state A are shown in Figure 7 and summarized in Table S6 (SI). For excited state A only one of the copper centers undergoes a geometric change from the ground state. A

18

bond length increase between Cu1 and N13 undergoes the greatest bond length change of 0.148

Å. Calculations predict no other major bond length changes between the ground state and excited

state A. The bond angle N2–Cu1–S25 at 132.3° in the ground state is decreased by 20.3° to become

112.0° in excited state A. This decrease in angle results in a less planar Cu1 metal center.

Photoinduced Jahn-Teller distortion for 3-coordinate Au(I) systems have been previously reported

wherein a trigonal planar center in the ground state is distorted to a T-shape upon excitation.[21] Our

excited state calculations are in agreement with this previous study. However, in our case only one

of the Cu centers undergoes this distortion, leaving the other Cu center unchanged. A single metal

ion transition is also observed in MO calculations of excited state A, shown in Figure S13 (SI).

Calculations indicate that a significant CuSCN→Py π^* transition occurs for a single Cu metal ion

center upon excitation at 318 nm. This MLCT transition is observed in the highest contributing

MO transition shown in Figure 8. Because of the single site geometric distortion and lone metal

MO transition, excitation at 318 nm most likely results in a mixed valence Cu(I)-Cu(II) complex.

Similar results have been reported on excited state computations for multinuclear Au(I) systems

by Bojan *et al.*[22] In this study optimization of the lowest excited triplet state of

$[Au_2\{(Ph_2Sb)_2O\}_3]^{2+}$ resulted in a Jahn-Teller distortion for a single Au center.[22] Distortion of both

centers resulted in destabilization of the excited triplet state.[22] Regardless, because emission

intensity reduction is not observed upon laser irradiation at energies corresponding to excited state

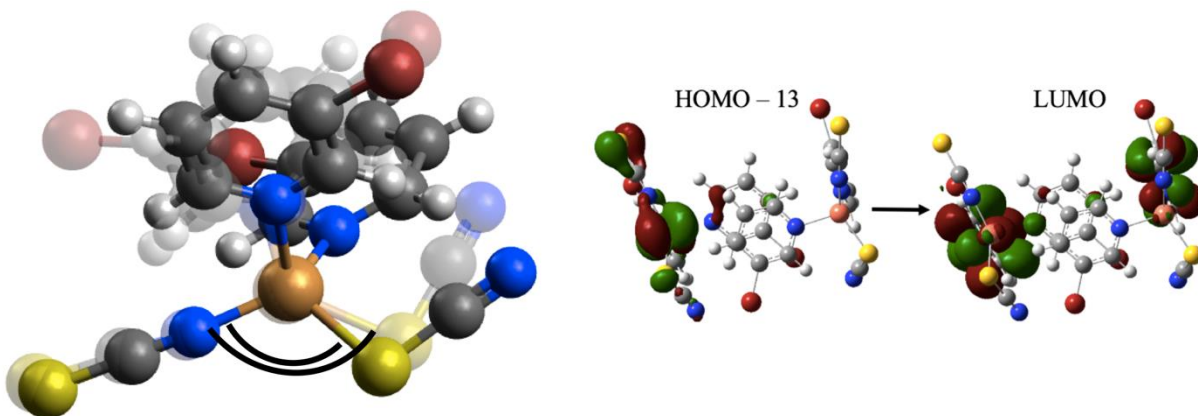A, we do not assign the lone MLCT transition to the mechanism responsible for optical memory.

Figure 7. Overlay of the single changed Cu center in excited state A and ground state (opaque) showing the predicted molecular change upon excitation at 318 nm. The physical change is a result of the the highest contributing MO transition shown from the HOMO-13 to the LUMO. This is a CuSCN→Py π^* transition that is in agreement with a MLCT. Second unchanged Cu center omitted for clarity.

We now turn our attention to TD-DFT calculations of a higher-energy-yet-more-relevant excited state B, which is of the most interest in explaining the phenomenon of optical memory observed in CuSCN(3-BrPy)$_2$. This excited state B occurs at a calculated energy of 271 nm and corresponds to the observed reduction of emission intensity upon experimental irradiation at 266 nm. A stark difference is observed between the MO calculation of excited state B and the previously mentioned excited state A. As shown in Figure 8, in this higher energy excited state, MO calculations indicate that the primary transition for excited state B is a CuSCN→C–Br σ^* electron transfer. Almost absent are any CuSCN→Py π^* transitions, previously observed in excited state A. In excited state B a significant C–Br bond length increase is predicted as the bond order decreases from C–Br σ^* population. Because this predicted change only occurs at the laser irradiation wavelength where emission intensity is reduced, we identify it as the main driver of optical memory behavior in CuSCN(3-BrPy)$_2$.
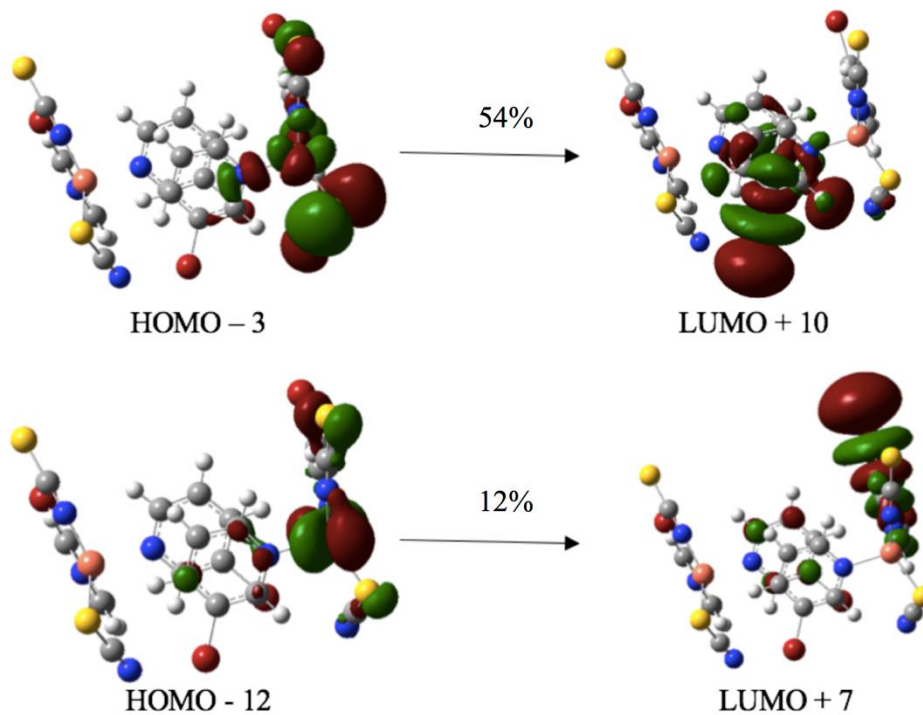
Figure 8. Two highest contributing orbital transitions of excited state B of {[Cu(SCN)$_2$(3-BrPy)$_2$] }$_2^{-2}$ at 271 nm showing only CuSCN→C-Br σ* transition.

We have also performed TD-DFT calculations of a {[Cu(SCN)$_2$(3-ClPy)$_2$] }$_2^{-2}$ model. The excitation spectrum is shown in Figure S16 (SI). As shown below in Figure 9, the transitions with the highest oscillator strengths correspond to transitions with MLCT character from the CuSCN backbone to the π* pyridine ring, similar to what is seen for the bromopyridine complex. It was found that both the calculated and the experimental results showed broad bands corresponding to MLCT from the CuSCN backbone to the Py π*. The orbitals corresponding to the transitions with the highest oscillator strength were mapped and used to determine the transition types. Orbital transitions shown above support the MLCT transition assignment wherein an electron from the CuSCN center is transferred to the aromatic π* system. Notably, absent from the Cl species is the presence of any significantly contributing CuSCN→C–Cl σ* transitions.
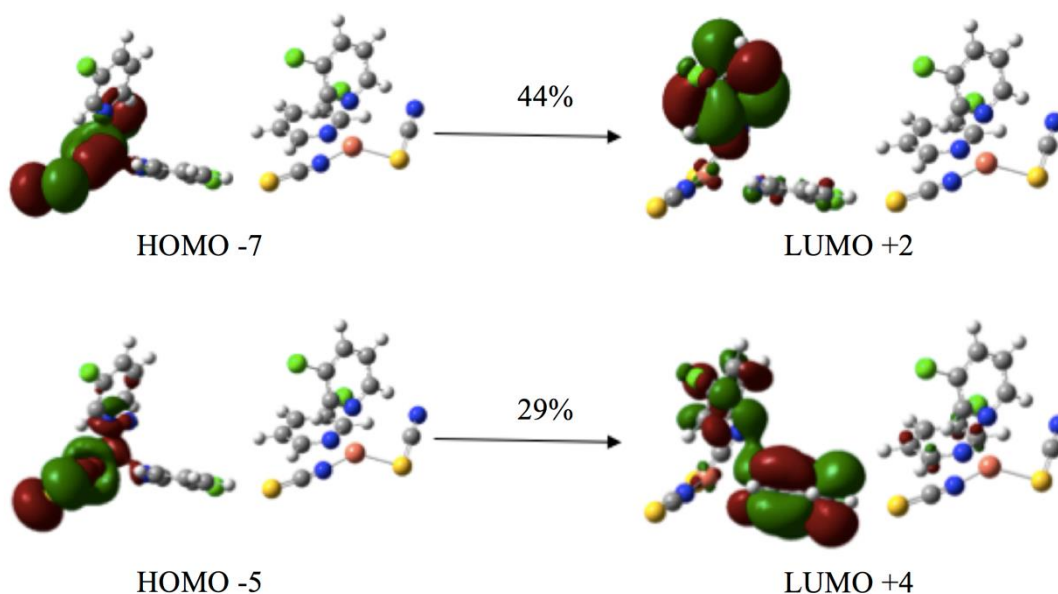
**Figure 9.** Two highest contributing orbital transitions of $\{[Cu(SCN)_2(3\text{-}BrPy)_2]\}_2^{-2}$ at 380 nm.

4. Optical Memory Mechanism

The observed decay in the luminescence of a $CuSCN(3\text{-}BrPy)_2$ single crystal indicates the creation of a non-luminescent species. If we initially assume that the Cu(I) is the primary photoreactive species, a possible mechanism involves electron transfer from Cu(I) to the excited state 3-BrPy ligand. Thus, we propose that laser irradiation at 266 nm of a $CuSCN(3\text{-}BrPy)_2$ unit within the polymer results in a reversible two-step photo-induced electron transfer resulting in oxidation of the Cu(I) center to Cu(II). The resulting non-luminescent Cu(II) species is consistent with the observed decrease of emission intensity during laser irradiation.

In step (1) a localized monomer unit of the $CuSCN(3\text{-}BrPy)_2$ polymer chain is excited by laser at 266 nm, resulting in initial formation of Cu(II) (shown in Scheme 2). Luminescence of CuSCN complexes coordinated with aromatic ligands results in an MLCT transition, whereby a Cu electron is transferred to the aromatic ring. In coordination complexes Cu(II) is a well-known luminescence quencher due to its intrinsic paramagnetic nature.[23-24] Occurrence of the Cu(I)/Cu(II) redox couple is energetically reasonable in the current case due to the modest standard reduction

potential ($E°$ for $Cu^{2+}/Cu^{+} \approx -0.16$ V).[25] Thus, we assign the loss of luminescence to the creation of a Cu(II) complex.

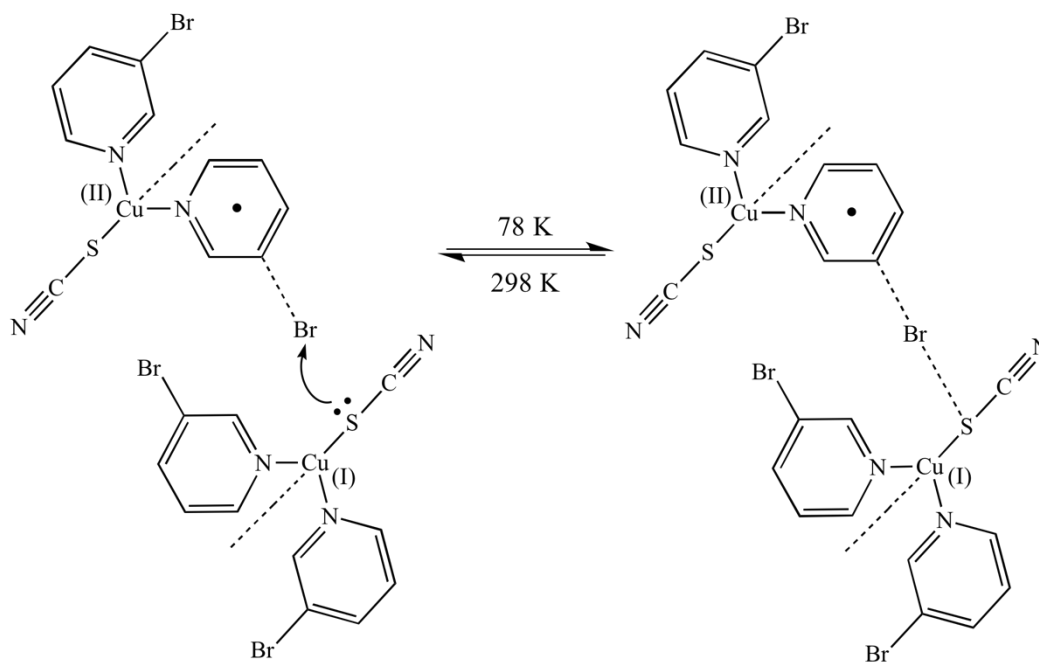**Scheme 2.** Step 1 of the photochemical reaction of $Cu^{(I)}SCN(3\text{-BrPy})_2$ wherein excitation of the Cu results in an electron transfer to the aromatic ligand and an elongation of the C–Br bond.

$$Cu^{(I)}SCN(3\text{-BrPy})_2 + h\nu \text{ (266 nm)} \rightarrow [Cu^{(II)}SCN(3\text{-BrPy}^{\bullet})(3\text{-BrPy})]^*$$
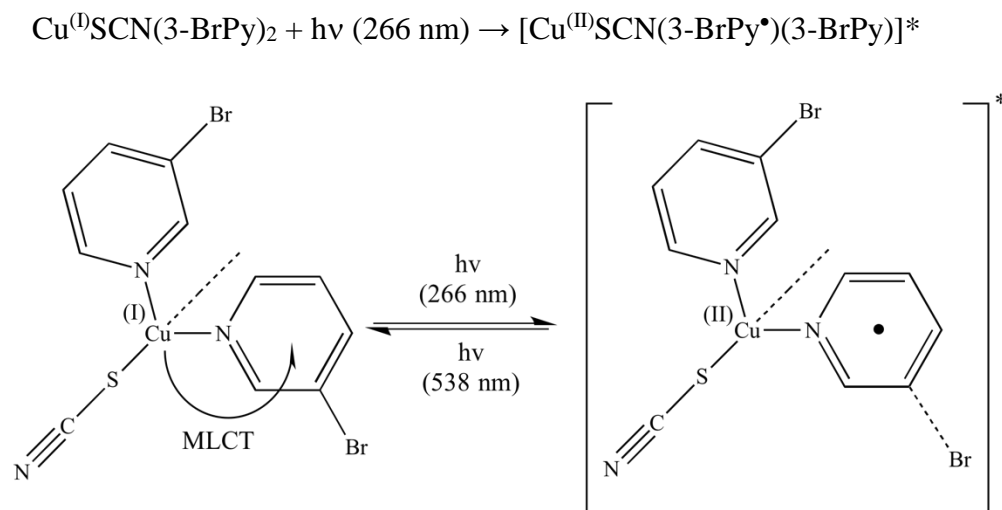
Because we observe no loss in luminescence intensity for the 3-ClPy species, we identify the C–Br bond as being responsible for step (2). This claim is further supported by the previously-mentioned DFT calculations that show only a C–Br bond length increase at 266 nm. Because it is a luminescent complex, we view excitation of $CuSCN(3\text{-BrPy})_2$ as completely reversible at all temperatures with relaxation occurring via the emission of light. Because the loss of emission can be maintained indefinitely simply by maintaining the temperature at 78 K, a second process must be occurring to inhibit the relaxation of $[Cu^{(II)}SCN(3\text{-BrPy})_2]^*$. In step (2) (shown in Scheme 3) we consider capture of the halogen by the neighboring SCN ligand on an adjacent chain. Previous experimental work by Rosokha et al. have demonstrated that halogens and pseudo halogens are able to form these complex interactions that are similar in strength to hydrogen bonds.[26]

Scheme 3. Step 2 of the photochemical reaction of $Cu^{(I)}SCN(3\text{-BrPy})_2$ where elongation of the C–Br bond allows donation of the S lone pair from the adjacent SCN ligand to the Br acceptor. A

23

metastable halogen bond is formed between the adjacent CuSCN(3-BrPy)$_2$ units preventing relaxation of the electron.

$$[Cu^{(II)}SCN(3\text{-}BrPy^{\bullet})(3\text{-}BrPy)]^* + CuSCN(3\text{-}BrPy)_2 \rightarrow CuSCN(3\text{-}BrPy)Py\cdots Br\cdots SCNCu(3\text{-}BrPy)_2$$

These halogen bonds are of intense interest due to the implications in the design of supramolecular structures.[26-32] The halogen bonding ability of SCN has been reported and has been described in terms of a Lewis acid/base reaction in which the C–Br σ* acts as an acceptor of an S-atom lone pair.[26,29-34] We describe this type of interaction in Figure 10 in terms of the molecular orbitals of CuSCN(3-BrPy)$_2$ and CuSCN(3-ClPy)$_2$. As shown in Figure 10, the lower energy of the C–Br σ* orbital allows for acceptance of the S lone pair, forming a stabilizing halogen bond between the heterocyclic aromatic ring and the SCN ligand. In the case of 3-ClPy, the C–Cl σ* energy is significantly higher, resulting in a destabilizing C–Cl⋯S interaction. Stabilization of this bridge is important because it locks the halogen atom in place irreversibly at low temperatures and prevents relaxation of the non-luminescent Cu(II) species back to luminescent Cu(I).
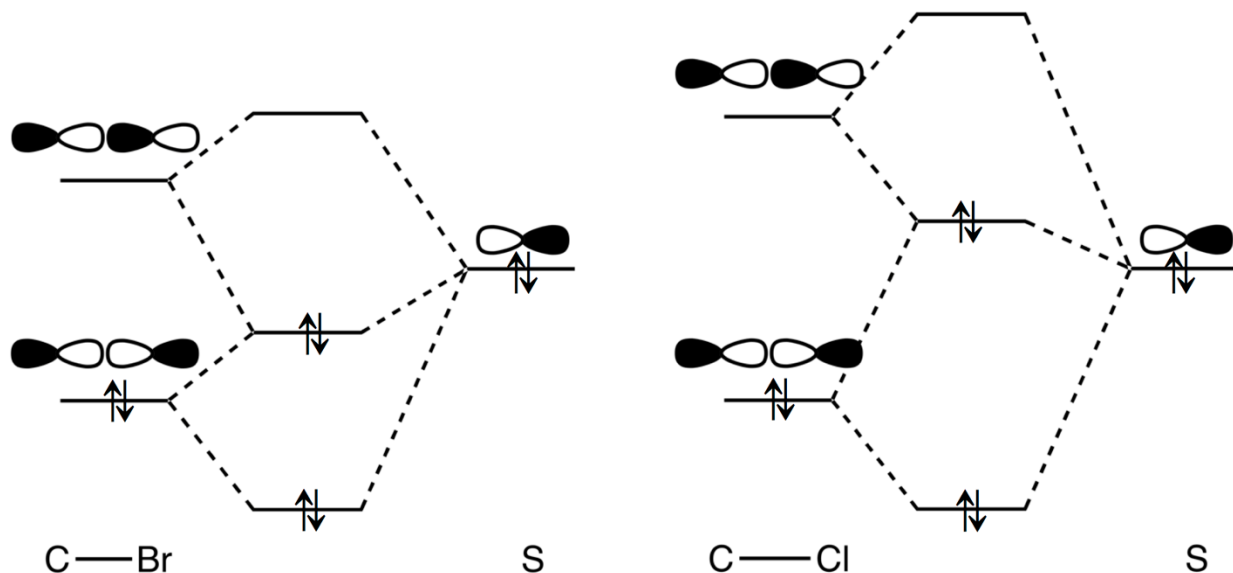
Figure 10. Molecular orbital interaction diagrams showing the C-Br mixing with the S lone pair to produce halogen bonding in $CuSCN(3\text{-}BrPy)_2$ crystals. The mixing of the C–Br σ^* with the S lone pair results in a stabilizing interaction, while the C–Cl σ^* results in a destabilizing interaction.

The work of Fourmigue has shown that SCN is able to form halogen bonding with an interaction preference at the sulfur end.[26] This preference for sulfur can be understood in terms of hard-soft acid-base chemistry[35] wherein strong halogen bonding is observed in Br/I⸱⸱S, Br⸱⸱Br, and I⸱⸱I systems that represent soft-soft interactions. Given the Lewis acid-base nature of halogen bonding, this conclusion is reasonable. It is important to note that halogen bonding would show two distinct angle preferences, depending on which end of SCN was involved. In X⸱⸱N bonding the X–N–C angle has been observed as being large, between 130º and 180º. Alternatively, in the case of X⸱⸱S bonding, the X–S–C angle is much smaller, between 90º and 110º. This angle difference arises from the orientation of the lone electron pairs of S and N.

To explore this halogen bond mechanism, we have performed a series of scan DFT single-point energy calculations for an adjacent pair of $CuSCN(3\text{-}BrPy)_2$ monomers. In this model, we

have manually moved the Br atom towards the neighboring SCN group. Because SCN is a linear group, we are able to define the Br atom movement within a Br–SCN plane. Migration is recorded as a function of C–Br distance, angle of movement towards the SCN group, and total energy of the system. Our calculations are presented in Figure 11. These calculations show a distinct saddle point as the Br migrates towards the central C atom with an increase in energy of 0.602 eV from the ground state. Upon further migration away from the Py ring, the Br atom falls into a local energy well with the local minimum located adjacent to the S atom. This S-atom preference is not surprising considering the expected soft-soft interaction and the preferred sharp angle of approach. Because of this halogen bond interaction at the local well, we expect a meta-stable state that has a reversible activation energy of 0.218 eV. This value is well below the available energy at 78 K and thus produces an irreversible reaction while at low temperatures. In fact, temperature dependence of halogen bonds has been observed previously, wherein halogen bonding was increased by lowering the temperature of solutions containing CBr_4 and $Bu_4N^+SCN^-$.[27]
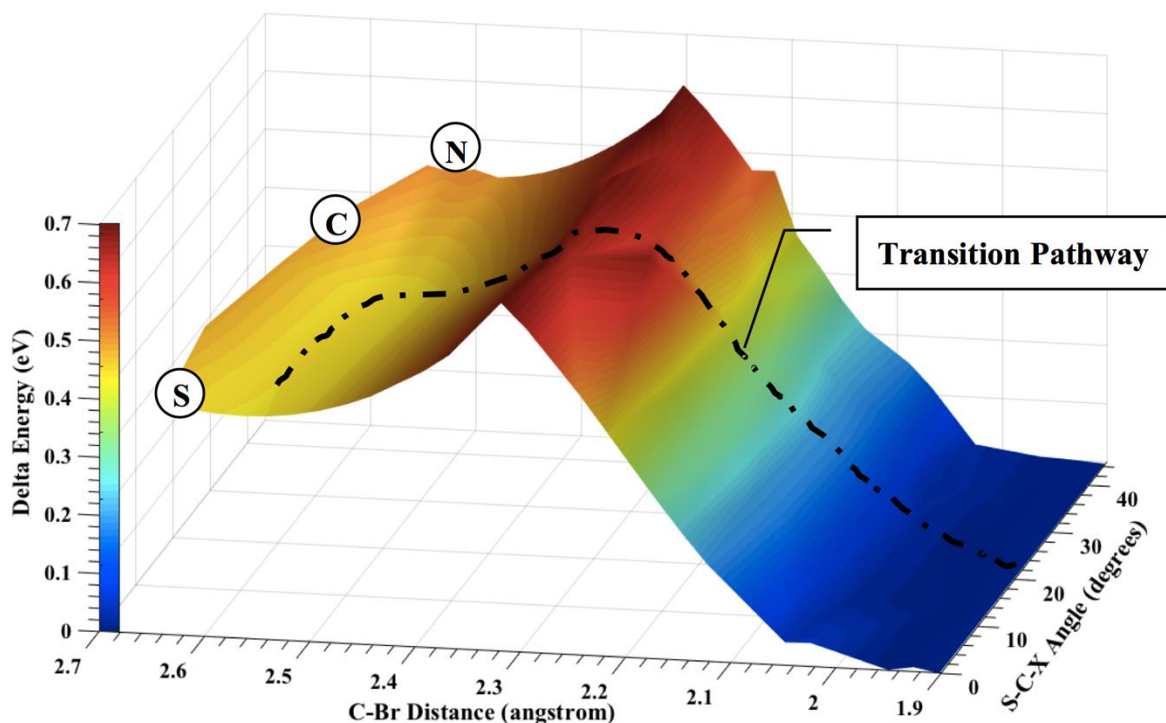
Figure 11. Single point energies of an adjacent pair of CuSCN(3-BrPy)$_2$ monomers as a function of the C–Br distance and angle. Relative S, C, and N location indicated for clarity.

5. Conclusion

In this study, we have synthesized the complexes CuSCN(3-BrPy)$_2$ and CuSCN(3-ClPy)$_2$ and investigated their structure and photochemical properties. with the structures contain independent 1-D $\cdots$CuSCN$\cdots$ chains, each decorated by pairs of 3-BrPy or 3-ClPy ligands coordinated at each metal center. The zig-zag chain results in close interactions between the Br and S atoms of the neighboring thiocyanate group. Laser irradiation at 266 nm and 78 K results in a reduction in luminescence intensity that increases with irradiation time. This luminescence intensity can be recovered by heating the sample to 298 K and re-cooling to 78 K, representing a formal write-erase sequence. This photochemical reaction has been assigned to a two-step electron transfer wherein the Cu(I) center is oxidized to a Cu(II) species with capture of the halogen by the neighboring SCN ligand of the adjacent chain. This interaction can be reversed by heating the sample to room temperature. Density functional calculations for inter-chain dimer models in the ground and various excited electronic states have provided reasonable explanations to the structural and optical results.

ASSOCIATED CONTENT

Supporting Information: The supporting information is available free of charge on the ACS Publications website. Additional crystallographic, spectral, and computational data (PDF). Crystallographic information on CCDC 1483473 and 1483474 can be obtained free of charge by e-mailing data_request@ccdc.cam.ac.uk or by contacting The Cambridge Crystallographic Data Centre, 12 Union Road, Cambridge, CB2 1EZ UK; Fax +44(0)1223-336033; www.ccdc.cam.ac.uk/data_request/cif.

AUTHOR INFORMATION

Corresponding Authors

*E-mail: howardp@maine.edu (H.H.P.).

*E-mail: omary@unt.edu (M.A.O.).

ACKNOWLEDGMENT

References

1. Tyson, D.; Bignozzi, C.; Castellano, F. Metal-Organic Approach to Binary Optical Memory. *J. Am. Chem. Soc*. **2002**, 124, 4562-4563.

2. Chan, J. C.-H.; Lam, W. H.; Yam, V. W.-W. A Highly Efficient Silole-Containing Diethienylethene with Excellent Thermal Stability and Fatigue Resistance: A Promising Candidate for Optical Memory Storage Materials. *J. Am. Chem. Soc.* **2014**, 136, 16994-16997.

3. Rath, S.; Heilig, M.; Port, H.; Wrachtrup, J. Periodic Organic Nanodot Patterns for Optical Memory. *Nano Lett*. **2007**, 7 (12), 3845-3848.

4. (a) Hollingsworth, G.; Barrie, J.; Dunn, B.; Zink, J. Optical Memory in Cu+-Doped / Beta"-Alumina. *J. Am. Chem. Soc.* **1988**, 110, 6569-6570. (b) Barrie, J.; Dunn, B.; Hollingsworth, G.; Zink, J. Optical Spectroscopy of Copper(I)-Doped Na+-Beta"-Alumina. *J. Phys. Chem.* **1989**, 93, 3958-3963. (c) Shin, K.; Barrie, J.; Dunn, B.; Zink, J. Optical Spectroscopy of Cu+/Ag+ Doped Beta"-Alumina. *J. Am. Chem. Soc. **1990**, 112, 5701-5706.*

5. (a) Hettiarachchi, S.; Patterson, H. "Write/Read/Erase" with Laser Irradiation of Dicyanoargentate(I) Doped and Pure Crystals. *J. Phys. Chem.* **2003**, 107, 14249-14254. (b) Li, X.; Pan, Z.; Baril-Robert, F.; Ahern, J.; Patterson, H. Novel Luminescent Heterobimetallic Nanoclusters of Copper(I), Silver(I), and Gold(I) Doped in Different Alkali Halide Crystals. *J. Phys. Chem. C.* **2014**, 118 (22), 11886-11894.

6. Li, X.; Pan, Z.; Welch, D.; Baril-Robert, F.; Pike, R.; Patterson, H. An Unusual Luminescent Anionic Copper(I) System: Dicyanocuprate(I) Ion in Nano and Bulky States. *J. Phys. Chem. C.* **2012**, 116, 26656-26667.

7. Omary, M.; Colis, J.; Larochelle, C. L.; Patterson, H. Optical Memory and Multistep Luminescence Thermochromism in Single Crystals of $K_2Na[Ag(CN)_2]_3$. *Inorg. Chem*. **2007**, 46 (10), 3798-3800.

8. Patterson, H.; Bourassa, J.; Shankle, G. Light-Induced Electron Transfer in Lead(II) Dicyanide. *Inorg. Chimica Acta.* **1994**, 226, 345-348.

9. Fischer, P.; Lucas, B.; Patterson, H.; Larochelle, C. Temperature Dependence of the Chemical Structure of $K_2Na[Ag(CN)_2]_3$. *Appl. Phys. A* **2002**, 74, S1B-S1298.

10. Fischer, P.; Lucas, B.; Omary, M.; Larochelle, C.; Patterson, H. Temperature Dependence of the Chemical Structure of $K_2Na[Ag(CN)_2]_3$ Tris[dicyanoargentate(I)] and the Role of Structural Phase Transitions. *J. Solid State Chem.* **2002**, 168, 267-274.

11. Larochelle, C.; Omary, M.; Patterson, H.; Fischer, P.; Fauth, P.; Allenpach, P.; Lucas, B.; Pattison, P. Optical, Synchrotron X-ray and Neutron Diffraction Investigations of Structural Changes in the Layered Compound $K_2Na[Ag(CN)_2]_3$. *Solid State Commun.* **2000**, 114, 155-160.

12. Miller, K.; McCullough, S.; Lepekhina, E.; Thibau, I.; Pike, R. Copper(I) Thiocyanate-Amine Networks: Synthesis, Structure, and Luminescence Behavior. *Inorg. Chem.* **2011**, 50, 7239-7249.

13. Graham, P. M.; Pike, R. D.; Sabat, M.; Baily, R. D.; Pennington, W. T. *Inorg. Chem.* **2000**, 39, 5121-5132.

14. (a) SMART Apex II, Data Collection Software, version 2.1; Bruker AXS Inc.: Madison, WI, 2005. (b) SAINT Plus, Data Reduction Software, version 7.34a; Bruker AXS Inc.: Madison, WI, 2005. (c) Sheldrick, G. M. SADABS; University of Göttingen: Göttingen, Germany, 2005. (d) Sheldrick, G. M. A Short History of SHELX. *ActaCryst.* **2008**, A64, 112-122.

15. Gaussian 09, Revision D.01, Frisch, M. J.; Trucks, G. W.; Schlegel, H. B.; Scuseria, G. E.; Robb, M. A.; Cheeseman, J. R.; Scalmani, G.; Barone, V.; Mennucci, B.; Petersson, G. A.; Nakatsuji, H.; Caricato, M.; Li, X.; Hratchian, H. P.; Izmaylov, A. F.; Bloino, J.; Zheng, G.; Sonnenberg, J. L.; Hada, M.; Ehara, M.; Toyota, K.; Fukuda, R.; Hasegawa, J.; Ishida, M.; Nakajima, T.; Honda, Y.; Kitao, O.; Nakai, H.; Vreven, T.; Montgomery, J. A.; Peralta, Jr., J. E.; Ogliaro, F.; Bearpark, M.; Heyd, J. J.; Brothers, E.; Kudin, K. N.; Staroverov, V. N.; Keith, T.; Kobayashi, R.; Normand, J.; Raghavachari, K.; Rendell, A.; Burant, J. C.; Iyengar, S. S.; Tomasi, J.; Cossi, M.; Rega, N.; Millam, J. M.; Klene, M.; Knox, J. E.; Cross, J. B.; Bakken, V.; Adamo, C.; Jaramillo, J.; Gomperts, R.; Stratmann, R. E.; Yazyev, O.; Austin, A. J.; Cammi, R.; Pomelli, C.; Ochterski, J. W.; Martin, R. L.; Morokuma, K.; Zakrzewski, V. G.; Voth, G. A.; Salvador, P.; Dannenberg, J. J.; Dapprich, S.; Daniels, A. D.; Farkas, O.; Foresman, J. B.; Ortiz, J. V.; Cioslowski, J.; Fox, D. J. Gaussian, Inc., Wallingford CT, 2010.

16. (a) Zhao, Y.; Truhlar, D. The M06 Suite of Density Functionals For Main Group Thermochemistry, Thermochemical Kinetics, Noncovalent Interactions, Excited States, And Transition Elements: Two New Functionals And Systematic Testing Of Four M06-Class Functionals And 12 Other Functionals. *Theor. Chem. Acc.* **2008**, 120, 215-241. (b) Zhao, Y.; Truhlar, D. Density Functionals with Broad Applicability in Chemistry. *Acc. Chem. Res.* **2008**, 41, 157-167. (c) Stevens, W.; Krauss, M.; Basch, H.; Jasien, P. Relativistic Compact Effective

Potentials and Efficient, Shared-Exponent Basis Sets for the Third-, Fourth-, and Fifth-Row Atoms. *Can. J. Chem.*, **1992**, 70, 612-630. (d) Cundari, T.; Stevens, W. Effective-Core-Potential Methods for the Lanthanides. *J. Chem. Phys.* **1993**, 98, 5555-5565.

17. Becke, A. D. Density-Functional Thermochemistry. III. The Role of Exact Exchange. *J. Chem. Phys.* **1993**,*98,* 5648-5652.

18. (a) Lee, C.; Yang, W.; Parr, R. G. Development of the Colle-Salvetti Correlation-Energy Formula into a Functional of the Electron Density. *Phys. Rev. B.* **1988**, 37785-37789. (b) Hay, P. J.; Wadt, W. R. Ab Initio Effective Core Potentials for Molecular Calculations - Potentials for the Transition-Metal Atoms Sc to Hg. *J. Chem. Phys.* **1985**, 82, 270-283. (c) Wadt, W. R.; Hay, P. J. Ab Initio Effective Core Potentials for Molecular Calculations - Potentials for Main Group Elements Na to Bi. *J. Chem. Phys.* **1985**, 82, 284-298. (d) Hay, P. J.; Wadt, W. R. Ab Initio Effective Core Potentials for Molecular Calculations - Potentials for K to Au Including the Outermost Core Orbitals. *J. Chem. Phys.* **1985**, 82, 299-310.

19. Healy, P.; Pakawatchai, C.; Papsergio, R.; Patrick, V.; White, A. Lewis Base Adducts of Group IB Metal(I) Compounds. 9. Synthesis and Crystal Structures of Adducts of Copper(I) Thiocyanate with Substituted Pyridine Bases. *Inorg. Chem. 1984, 23, 3769-3776.*

20. (a) Lobana, T.; Sharma, R.; Hundal, G.; Butcher, R. Synthesis of 1D $\{Cu_6(\mu_3\text{-}SC_3H_6N_2)4(\mu\text{-}SC_3H_6N_2)_2(\mu\text{-}I)_2I_4\}_n$ and 3D $\{Cu_2(\mu\text{-}SC_3H_6N_2)_2(\mu\text{-}SCN)_2\}_n$ Polymers with 1,3-Imidazolidine-2-thione: Bond Isomerism in Polymers. *Inorg. Chem.* **2006**, 45, 9402-9409. (b) Toeniskoetter, R.; Solomon, S. Infrared Spectra of Copper Thiocyanate Complexes. *Inorg. Chem.* **1968**, 7, 617-620.

21. Barakat, K.; Cundari, T.; Omary, M. Jahn-Teller Distortion in the Phosphorescent Excited State of Three-Coordinate Au(I) Phosphine Complexes. *J. Am. Chem. Soc.* **2003**, 125, 14228-14229.

22. Bojan, V.; Fernandez, E.; Laguna, A.; Lopez-de-Luzuriage, J.; Monge, M.; Olmos, E.; Silvestru, C. Phosphorescent Excited State of $[Au_2\{(Ph_2Sb)_2O\}_3]^{2+}$: Jahn-Teller Distortion at Only One Gold(I) Center. *J. Am. Chem. Soc.* **2005**, 127, 11564-11565.

23. (a) Ruan, Y.; Li, C.; Tang, J.; Xie, J. Highly Sensitive Naked-Eye and Fluorescence "Turn-On" Detection of Cu^{2+} Using Fenton Reaction Assisted Signal Amplification. *Chem. Commun.* **2010**, 46, 9220-9222. (b) Bergonzi, R.; Fabbrizzi, L.; Licchelli, M.; Mangano, C. Molecular Switches of Fluorescence Operating Through Metal Centred Redox Couples. *Coord. Chem. Rev.* **1998**, 170, 31-46. (c) Lee, Y.; Kubota, E.; Fuyuhiro, A.; Kawata, S.; Harrowfield, J.; Kim, Y.; Hayami, S. Synthesis, Structure and Luminescence Properties of Cu(II), Zn(II) and Cd(II) Complexes with 4′-Terphenylterpyridine. *Dalton Trans.* **2012**, 41, 10825-10831.

24. Harris, D. C. Quantitative Chemical Analysis, 7th ed.; W. H. Freeman and Company: New York, New York, 2007.

25. Cauliez, P.; Roisnel, T.; Llusar, R.; Fourmigue, M. The Thiocyanate Anion as a Polydentate Halogen Bond Acceptor. *CrystEngComm.* **2010**, 12, 558-566.

26. Rosokha, S. V.; Neretin, I.; Rosokha, T.; Hecht, J.; Kochi, J. Charge-Transfer Character of Halogen Bonding: Molecular Structures and Electronic Spectroscopy of Carbon Tetrabromideand Bromoform Complexes with Organic σ - and π -Donors. *Heteratom Chem.* **2006**, 17 (5), 449-459.

27. Herve, K.; Cador, O.; Golhen, S.; Costuas, K.; Halet, J.; Shirahata, T.; Muto, T.; Imakubo, T.; Miyazaki, A.; Ouahab, L. Iodine Substituted Tetrathiafulvalene Radical Cation Salts with $[M(isoq)_2(NCS)_4]^-$ Anions where $M = Cr^{III}$, Ga^{III}: Role of I···S and S···S Contacts on Structural and Magnetic Properties. *Chem. Mater.* **2006**, 18, 790-797.

28. Fourmigue, M.; Auban-Senzier, P. Anionic Layered Networks Reconstructed from $[Cd(SCN)_3]_\infty^-$ Chains in Pseudo One-Dimensional Conducting Salts of Halogenated Tetrathiafulvalenes. *Inorg. Chem.* **2008**, 47, 9979-9986.

29. Rosokha, S.; Kochi, J. X-ray Structures and Electronic Spectra of the π-Halogen Complexes between Halogen Donors and Acceptors with π-Receptors. In Halogen Bonding: Fundamentals and Applications; Metrangolo, P., G., R., Eds.; Springer Berlin Heidelberg: Berlin, 2008; Vol. 126, pp 137-160.

30. Metrangolo, P.; Resnati, G.; Pilati, T.; Biella, S. Halogen Bonding in Crystal Engineering. In Halogen Bonding: Fundamentals and Applications; Springer Berlin Heidelberg: Berlin, 2008; Vol. 126, pp 105-136.

31. Ranganathan, A.; El-Ghayoury, A.; Meziere, C.; Harte, E.; Clerac, R.; Batail, P. Balancing Framework Densification with Charged, Halogen-Bonded-π-Conjugated Linkages: $[PPh_4]_2[EDT-TTF–I]_2\{[EDT-TTF–I][Re_6Se_8(CN)_6]\}$. *Chem. Comm.* **2006**, 27, 2878-2880.

32. Bock, H.; Holl, S. Interaction in Molecular Crystals, 181. σ-Donor/Acceptor Complexes $M_AI_4···X^-$ ($X = Br^-$, I^-, SCN^-) of Tetraiodo Acceptor Molecules M_AI_4 (M_A = Ethene, Thiophene, N-Methylpyrrole) in Tetraphenylphosphonium Halide Salts. *Z. Naturforsch.* **2002**, 57b, 843-858.

33. Bock, H.; Holl, S. Interaction in Molecular Crystals, 180. σ-Donor/Acceptor Complexes S(CI)$_4$···X$^-$ (X = I$^-$, SCN$^-$) of Tetraiodothiophene in Tetra(n-butyl)ammonium Halide Salts. *Z. Naturforsch*. **2002**, 57b, 835-842.

34. Bock, H.; Holl, S. Interaction in Molecular Crystals, 179. σ-Donor/Acceptor Complexes I$_2$C=CI$_2$···X$^-$ (X$^-$ = Cl$^-$, Br$^-$, I$^-$, SCN$^-$) of Tetraiodoethene in Tetra(n-butyl)ammonium Halide Salts. *Z. Naturforsch*. **2002**, 57b, 713-725.

35. Pearson, R. G. (Ed.), 1973, Hard and Soft Acids and Bases. Dowden, Hutchinson & Ross, Stroudsburg, PA.
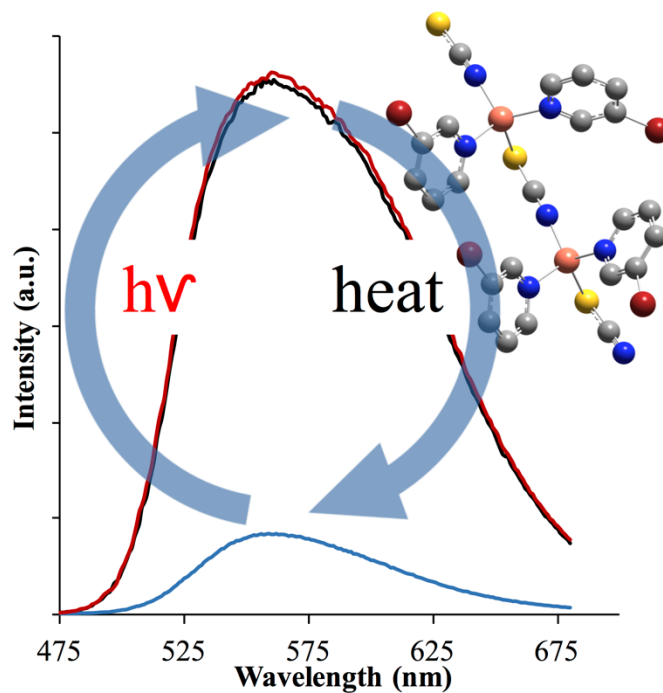
TOC Synopsis

A "write/erase" optical memory behavior is reported herein for $\{CuSCN(3\text{-}XPy)_2\}_n$ coordination-polymer chains, X = Br; Cl. Intense MLCT emission is observed for both complexes at 77 K. Emission intensity for $CuSCN(3\text{-}BrPy)_2\}_n$ is reduced upon 266 nm laser irradiation, whereas $CuSCN(3\text{-}ClPy)_2\}_n$ remains unchanged. Warming and recooling the Br complex restores emission intensities. Using DFT, a two-step photochemical electron transfer mechanism is proposed whereby the Br atom migrates towards and is captured by an adjacent SCN ligand.